Chiral Bloch oscillation and nontrivial topology in a ladder lattice with magnetic flux

Yi Zheng, Shiping Feng, and Shi-Jie Yang

Phys. Rev. A **96**, 063613 — Published 12 December 2017

DOI: 10.1103/PhysRevA.96.063613

Chiral Bloch oscillation and nontrivial topology in a ladder lattice with magnetic flux

Yi Zheng, Shiping Feng, and Shi-Jie Yang*
Department of Physics, Beijing Normal University, Beijing 100875, China

Bloch oscillations in a tilted ladder lattice are studied in the presence of artificial magnetic flux. The oscillations exhibit chiral characteristics which may be used to distinguish the Meissner phase and the vortex phase. By incorporating the diagonal hopping into the ladder, the dynamical evolution reveals a phase transition as the diagonal hopping rate exceeds a critical value. The pseudospin polarization rotates a full circle in a Bloch oscillating period which implies nontrivial topology of the system. At the critical point, the lowest band gap is closed and the wave packet propagates alternatively in the two bands that leads to a doubled Bloch period. Edge states arise in the region of nontrivial band topology even in the absence of chiral symmetry. Our study may provide a dynamical way to identify the quantum phases and topological transitions in the condensed matter physics.

PACS numbers: 67.85.-d, 03.65.Vf, 03.75.Lm

I. INTRODUCTION

The experimental realization of tunable artificial gauge fields in optical lattices have enabled the quantum simulation of Hofstadter-Harper Hamiltonian with ultracold atoms[1–3]. A quantized magnetic flux penetrating a two-dimensional (2D) lattice system can be mimicked by applying laser-assisted tunneling effect[4–6]. In finite systems, such model has intrigued the exploration of topological insulating states[7], quantum Hall chiral edge states[8], and spin-orbit (SO) coupling[9], *etc*[10].

A two-leg ladder lattice subjected to a synthetic magnetic field shares the basic properties of the 2D Hofstadter-Harper Hamiltonian, which has attracted extensive theoretical and experimental investigations[11–21]. Regarding the left-right leg degrees of freedom as a pseudospin, this model has been shown to possess the essence of SO coupling, which locks the spin and the momentum[16, 17]. The energy band structure of the ladder is analogous to that of a one-dimensional (1D) SO coupled system[22]. The ground state properties in the non-interacting region reveal the chiral Meissner currents in the presence of an artificial magnetic field. A saturation of the current occurs at the quantum phase transition point between the Meissner phase and the vortex phase[16, 17].

Most previous studies concerning the ladder systems in the presence of a synthetic magnetic field are focused on the ground state or low-energy excitations. Dynamical features have attracted less attentions. When a small gradient field is applied along the legs of the ladder system, we expect a wave packet evolve as Bloch oscillation (BO). The dynamics of BO have been shown to be distinctive in the presence of SO coupling[23]. Thus the BOs should be strongly influenced by the synthetic magnetic field.

In this paper, we study the dynamical processes of the bosonic ladder system which is subjected to a synthetic magnetic field and a static linear force. It shows that the BOs exhibit chiral currents. We also demonstrate that the quantum phase transition between the Meissner phase and the vortex phase can be clearly identified by this dynamical way. In the presence of diagonal tunnelings, band crossing at the edges of the Brillouin zone (BZ) appears at a particular condition and a topological phase transition occurs. The total pseudospin polarization rotates a full circle in a BO period and the BO period doubles at the critical point. We explicitly examine the underling physics of the topological transition.

The paper is organized as follows. In section II, we describe formulism of the ladder system with artificial gauge field and a linear force. The chiral Bloch oscillations with and without diagonal tunneling are presented in section III and IV, respectively. In section V, we analyse the evolution of an eigenstate in momentum space. The band topology, as well as edge states with and without chiral symmetry are demonstrated in section VI. The discussion and summary are included in section VII.

II. FORMULISM

The non-interacting bosonic ladder system is described by the tunneling terms of the Bose-Hubbard model. With a magnetic flux $\Phi = 2\phi$ per plaquette piercing the system as well as a small gradient field applying along the legs, the Hamiltonian is

$$\begin{aligned} H_0 = & - t_{\parallel} \sum_j (e^{-i\phi} a_{j+1}^{\dagger} a_j + e^{i\phi} b_{j+1}^{\dagger} b_j) \\ & - t_{\perp} \sum_j a_j^{\dagger} b_j + \text{H.c.} + F_0 \sum_j j n_j . \end{aligned} \tag{1}$$

Here a_j (b_j) represents the bosonic annihilation operator acting on site j in the left (right) leg. The first two terms are the tunnelings along the legs and the third term is the tunneling across the rung, with hopping rates $t_{\parallel}$ and $t_{\perp}$, respectively. F_0 is the gradient caused by the

*Corresponding author: yangshijie@tsinghua.org.cn

static linear force. $n_j = a_j^\dagger a_j + b_j^\dagger b_j$ is the number operator for site j. Here a Landau gauge is chosen, which ensure a translation symmetry along the leg direction. The choice of gauge does not affect observable quantities such as the chiral current in the ground state[21], the quench dynamics[24], *etc.* Regarding the left-right leg degree of freedom as a pseudo-spin, Eq.(1) is mapped onto a SO coupled system. By making a Fourier transform $o_j^\dagger = \frac{1}{\sqrt{L}}\sum_k e^{-ikj} o_k^\dagger$ with $o_{j(k)}^\dagger = [a_{j(k)}^\dagger, b_{j(k)}^\dagger]$ and L the number of sites along the legs, we arrive at the Hamiltonian in momentum space

$$H_0(k) = -t_\parallel \sum_k o_k^\dagger \mathcal{H}(k) o_k, \tag{2}$$

where

$$\mathcal{H}(k) = \begin{bmatrix} \varepsilon(k) - \kappa(k) & \tau \\ \tau & \varepsilon(k) + \kappa(k) \end{bmatrix} + iF \begin{bmatrix} -\frac{d}{dk} & \\ & -\frac{d}{dk} \end{bmatrix}. \tag{3}$$

The first matrix describes an effective SO coupling induced by the nonzero flux[25]. Here we have set $\varepsilon(k) = 2\cos\phi\cos k$, $\kappa(k) = 2\sin\phi\sin k$, $\tau = t_\perp/t_\parallel$ and $F = F_0/t_\parallel$. When $k \to 0$, $\varepsilon(k)$ represents the kinetic energy plus an energy shift, both multiplied by a coefficient which is related to the flux. $\kappa(k)$ approaches the momentum k multiplied by $2\sin\phi$ which can be viewed as the coupling strength.

We assume $F = 0$ to get some basic features about the system. A two-band spectrum yield (in unit of $t_\parallel$),

$$E_\pm(k) = -\varepsilon(k) \pm \sqrt{\kappa^2(k) + \tau^2}, \tag{4}$$

which are symmetric about $k = 0$ [16, 26, 27] and do not cross each other unless $t_\perp = 0$. The two local minima of $E_-(k)$, locating at $\sin k_{c\pm} = \pm\sin\phi\sqrt{1 - \tau^2/\tau_c^2}$, can merge at $k = 0$ when $\tau = \tau_c = 2\sin^2\phi/\cos\phi$. Only one minimum $E_-(k = 0)$ exists for $\tau \geq \tau_c$ or equivalently, $\phi \leq \phi_c = \arccos\left[-\tau/4 + \sqrt{\tau^2/16 + 1}\right]$. In such case, the ground state exhibits a Meissner phase which is characterized by the chiral current resembling the Meissner current to screen the magnetic field[11].

The presence of nonzero F breaks the discrete translation symmetry and the ground state properties for a finite size system become intricate. To avoid significant modification of the band dispersion, we assume a small linear force $F \ll 1$ which supports the BO. Eq.(2) is diagonalized as

$$H_0(k) = \sum_k \alpha_k^\dagger (E_- + iF\frac{d}{dk})\alpha_k + \beta_k^\dagger (E_+ + iF\frac{d}{dk})\beta_k, \tag{5}$$

where we have defined the creation operators of quasiparticles

$$\alpha_k^\dagger = \cos\theta_k a_k^\dagger + \sin\theta_k b_k^\dagger, \;\; \beta_k^\dagger = \sin\theta_k a_k^\dagger - \cos\theta_k b_k^\dagger, \tag{6}$$

with θ_k satisfying

$$\cos 2\theta_k \cdot \tau + \sin 2\theta_k \cdot \kappa(k) = 0. \tag{7}$$

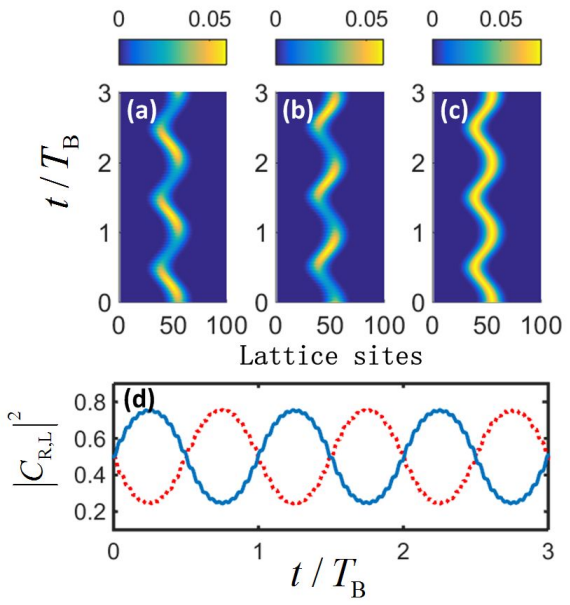

FIG. 1: (Color online) Oscillatory mode of a Gaussian wave packet under the influence of magnetic flux in the regime of the Meissner phase. (a-c) The density evolution in the left leg $|c_{Lj}(t)|^2$, the right leg $|c_{Rj}(t)|^2$ and the sum $|c_{totj}(t)|^2$, respectively. (d) displays the temporal evolution of the density fraction in the left (blue solid curve) and the right (red dotted curve) legs. The system parameters are $\tau = 2$, $\Phi = 0.4\pi$ and $F = 0.2$. The initial Gaussian wave packet is characterized by $\lambda = 10$, $k_0 = 0$ and $j_0 = 55$.

Eq.(5) represents two BO modes which correspond to the separating bands $E_\mp(k)$ respectively. Regarding to the lower band, the quasi-momentum of an eigenstate follows the classical equation of motion[28, 29]

$$k(t) = k_0 - Ft, \tag{8}$$

with k_0 the momentum of an initial state.

At the center (edges) of the BZ, $\alpha_{0(\pm\pi)}^\dagger = \frac{\sqrt{2}}{2}a_{0(\pm\pi)}^\dagger + \frac{\sqrt{2}}{2}b_{0(\pm\pi)}^\dagger$ (as reflected from Fig.1(d)), which can also be deduced from the $\sigma_x\mathcal{P}$ and $\sigma_x\mathcal{T}$ symmetry of Eq.(1), where σ_x gives rise to the mapping $a_j^\dagger(a_j) \leftrightarrow b_j^\dagger(b_j)$, $\mathcal{P}$ and $\mathcal{T}$ are respectively the parity operator ($\mathcal{P}a_j^\dagger = a_{-j}^\dagger$) and the time reversal operator ($\mathcal{T}a_j^\dagger = a_j$). By performing the Fourier transform, we arrive at $\mathcal{P}a_k^\dagger = \mathcal{T}a_k^\dagger = a_{-k}^\dagger$. Thus when $k = 0, \pm\pi$, $\sigma_x\mathcal{P}(c_1 a_k^\dagger + c_2 b_k^\dagger)|0\rangle = (c_1 b_k^\dagger + c_2 a_k^\dagger)|0\rangle = (c_1 a_k^\dagger + c_2 b_k^\dagger)|0\rangle$, which means $c_1 = c_2$. A Gaussian wave packet $|\psi\rangle$ centering at j_0 performs an oscillating mode with negligible inter-band coupling. We set the initial wave packet $|\psi(t=0)\rangle = \sum_j c_j(a_j^\dagger + b_j^\dagger)|0\rangle$ with $c_j = g\exp\left[-(j-j_0)^2/\lambda^2 + ik_0 j\right]$, where g is the normalizing factor, λ represents the width of the wave packet and $k_0 = 0, \pm\pi$. Since the group velocity is expressed as $v_g = [\partial E_-(k)/\partial k]_{k(t)}$, the center of the wave

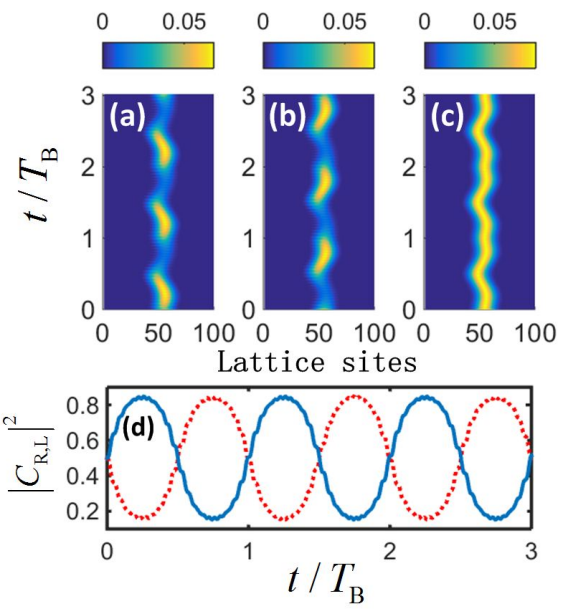

FIG. 2: (Color online) (a-c) The same as in the fig.1 in the regime of the vortex phase with $\tau = 2$, $\Phi = 0.8\pi$ and $F = 0.2$. There appears a rollback in each Bloch period in the total density evolution (c). (d) The density fraction in the left (blue solid curve) and the right (red dotted curve) legs.

packet evolves as[23]

$$j_c(t) = j_0 + \frac{1}{F}\left[E_-(k_0) - E_-(k_0 - F\cdot t)\right], \qquad (9)$$

which has the period of $T_{\rm B} = 2\pi/F$.

III. CHIRAL BLOCH OSCILLATION

The evolving wave packet can be depicted by the state $|\psi(t)\rangle = \sum_j \left[c_{{\rm L}j}(t)a_j^\dagger + c_{{\rm R}j}(t)b_j^\dagger\right]|0\rangle$. The features of the motion are captured by the probability amplitudes $c_{{\rm L}j}(t)$ and $c_{{\rm R}j}(t)$. We define $|c_{{\rm tot}j}(t)|^2 = |c_{{\rm L}j}(t)|^2 + |c_{{\rm R}j}(t)|^2$ to describe the total density distribution of the two distinguishable chains. The number fraction in each chain is characterized by $|C_{\rm L}(t)|^2 = \sum_j |c_{{\rm L}j}(t)|^2$ and $|C_{\rm R}(t)|^2 = \sum_j |c_{{\rm R}j}(t)|^2$. Figure 1 shows the evolving trajectories of the density distributions for parameters favoring the Meissner phase, *e.g.*, $\tau = 2$ and $\Phi = 0.4\pi$, the wave packet is initialized by $\lambda = 10$ and $k_0 = 0$. All of $|c_{\sigma j}|^2$ ($\sigma = {\rm L}, {\rm R}, {\rm tot}$) exhibit the oscillating mode of BO (Fig.1(a)(b)(c)). We formulate the trajectory of the wave packet center with $j_c(t) = \sum_j j|c_{{\rm tot}j}|^2$ as displayed in Fig.3(a). The Bloch oscillation exhibits distinct chiral characteristics: the wave packet mainly populates the left leg when moving downward in the first half of BO period and tunnels to the the right leg when moving upward in the second half of BO period (see Fig.1(d)). This chiral current characteristics results from

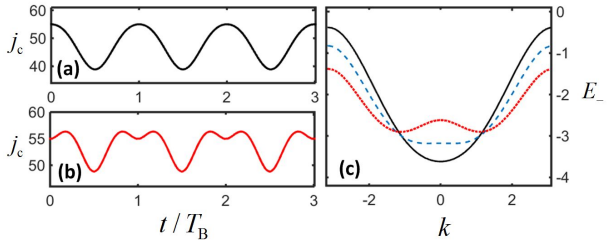

FIG. 3: (Color online) (a,b) Dissimilar trajectories of the center of the Gaussian wave packet in fig.1 and fig.2, respectively. (c) The lowest energy spectra of the Meissner phase (black solid) for $\tau = 2$ and $\Phi = 0.4\pi$ and the vortex phase (red dotted) for $\tau = 2$ and $\Phi = 0.8\pi$. In the latter case there is a hump near $k = 0$ which leads to the rollback in the curve of (b). The blue dashed curve is the energy spectrum at the transition point.

the spin-momentum locking of the SO coupling effect. From Eq.(2) and Eq.(3), the states with positive (negative) momentum tends to occupy the right (left) leg to lower the total energy.

On the other hand, when the parameters are in the vortex phase region, the initial direction of motion differs to the Meissner phase case, as shown in Fig.2 and Fig.3(b). At time $t = nT_{\rm B}$ ($n = 0, 1, 2...$), the state returns to $|k(t) = 0\rangle$ with $v_g = 0$, implying that the acceleration for the two cases have opposite signs. From Eq.(8) and the expression of v_g, we get the acceleration

$$a_c(t) \equiv \frac{\partial^2 j_c(t)}{\partial t^2} = -F\left[\frac{\partial^2 E_-(k)}{\partial k^2}\right]_{k(t)}, \qquad (10)$$

which is proportional to the curvature of the band E_- at $k(t)$. Figure 3(c) shows that the curvatures at $k = 0$ for the bands corresponding to the Meissner phase (black solid curve) and the vortex phase (red dotted curve) have different signs. At the transition point ($\tau = 2$, $\Phi = 2\arccos(\frac{\sqrt{5}-1}{2})$), the curvature vanishes, as specified by the dashed blue curve.

By making use of the relation (10), one can identify the phase diagram by the dynamical process. In Fig.4, we scan the values of $|a_c(t = T_{\rm B})|$ in the parameter space to obtain the phase boundary where $a_c(t = nT_{\rm B}) = 0$ ($n = 0, 1, 2...$). $a_c < 0$ corresponds to the Meissner phase whereas $a_c > 0$ the vortex phase. Our dynamical identification of the phase boundary is in agreement with the theoretical result $\tau = \tau_c$, as indicated by the red dashed curve in Fig.4.

IV. DYNAMICS WITH DIAGONAL COUPLING

We turn to investigate the effect of diagonal tunneling which couples the two chains with one site shifted. The

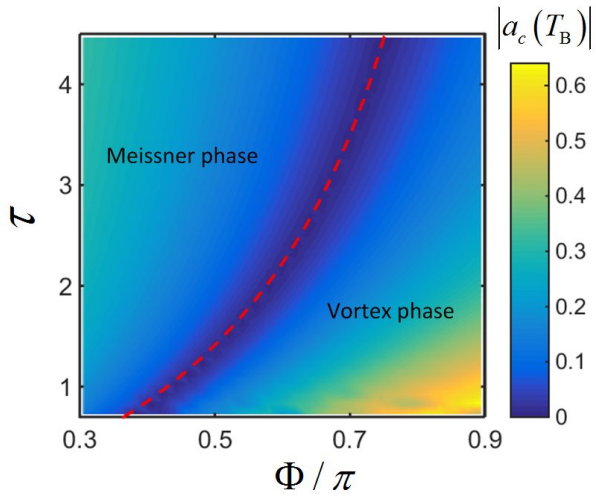

FIG. 4: (Color online) The phase diagram obtained by scanning the value of $|a_c(T_B)|$ in unit of $1/T_B^2$. The phase boundary is determined by $a_c(T_B) = 0$ which coincides with the theoretical prediction (red dashed curve).

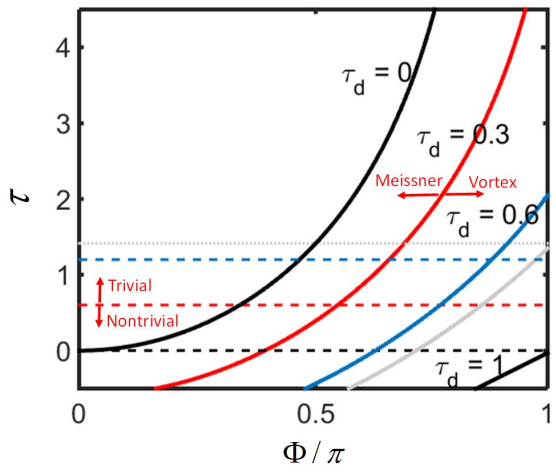

FIG. 5: (Color online) Solid curves: theoretical phase boundaries between the Meissner phase and the vortex phase calculated by Eq.(13) for $\tau_d = 0, 0.3, 0.6, 1$ as labeled in the diagram. Dashed lines ($\tau = 2\tau_d$): the topological trivial, nontrivial boundaries for different values of τ_d (black (lower) for $\tau_d = 0$, red (middle) for $\tau_d = 0.3$, blue (upper) for $\tau_d = 0.6$). The left (right) side of the solid curves correspond to the Meissner (vortex) phase. The upper (lower) area of the dashed lines correspond to the topological trivial (nontrivial) phase. The case for $\tau_d = \sqrt{2}/2$ is labeled by the gray solid curve and the gray dotted line, where the trivial vortex phase starts to vanish. The entire vortex phase disappears as $\tau_d > 1$.

total Hamiltonian is $H = H_0 + H_d$, where

$$H_d = -t_d \sum_j \left[(a_j^\dagger b_{j+1} + a_{j+1}^\dagger b_j) + \text{H.c.} \right]. \tag{11}$$

By replacing τ with $\tilde{\tau}(k) = \tau + 2\tau_d \cos k$ ($\tau_d = t_d/t_\parallel$), we obtain the Hamiltonian matrix and the band structure with respectively the same form of Eq.(3) and Eq.(4). The quasi-particle creation operators also remain the same as in Eq.(6) while θ_k is determined by

$$\tan 2\theta_k = -\frac{\tau + 2\tau_d \cos k}{\kappa(k)}. \tag{12}$$

The boundary between the Meissner phase and the vortex phase is then shifted to

$$\tau_c' = 2\left(\frac{\sin^2 \phi}{\cos \phi + \tau_d} - \tau_d \right), \tag{13}$$

which recovers the former case at $\tau_d = 0$. The vortex phase shrinks with the increase of τ_d as displayed in Fig.5. For positive τ, the vortex phase disappears as long as $\tau_d \geq 1$.

The presence of diagonal coupling induces a topological transition in the ladder system[16] which can be definitely revealed by the dynamical evolution. By defining the total pseudospin polarization $\mathbf{S} = \sum_j \mathbf{S}_j$, where the local pseudospin $\mathbf{S}_j(t) = \psi_j^\dagger(t)\hat{\sigma}\psi_j(t)$ with $\psi_j^\dagger(t) = \left[c_{\text{L}j}^*(t), c_{\text{R}j}^*(t)\right]$, one can map the evolving states to a moving point on the Bloch sphere. Since the BO represents a quasi-momentum state evolving along the band, such mapping also reflects the information about the band structure. For separated two bands, $\sigma_x \mathcal{P}|k\rangle = \sigma_x|k\rangle = |k\rangle$ is satisfied when $k = 0, \pm\pi$, which indicates $S_z = 0$ in such cases. However, band crossing occurs at $k = \pm\pi$ when $\tau_d = \tau/2$. The eigenstates with quasi-momentum $k = \pm\pi$ become distinguishing and hence $\sigma_x \mathcal{P}|k\rangle = \sigma_x|-k\rangle = |k\rangle$ which means $S_z(k) = -S_z(-k)$. As a result, the wave packet switches to the second band from $|k = (-\pi)^+\rangle_-$ to $|k = \pi^-\rangle_+$ when reaching one edge of the BZ (see section V). The subsequent motion in the second band lasts T_B until it arrives at the other edge of the BZ and switches back to the lower band from $|k = (-\pi)^+\rangle_+$ to $|k = \pi^-\rangle_-$. Consequently, the period of such BO doubles as shown in Fig.6(a-d). On the other hand, such effect can be understood by the doubling of the BZ, which stem from the halving of the original unit cell. This point will be emphasized in sectionVI. Note that $|C_{\text{L,R}}|^2$ can reach the maximum 1 at respectively $t = (2n + 1/2)T_\text{B}$ and $t = (2n + 3/2)T_\text{B}$ ($n = 0, 1, 2, ...$).

For $\tau_d > \tau/2$, the bands reopen and the BO period recovers T_B (see Fig.6(f, g)). However, $|C_{\text{L,R}}(t)|^2 = 1$ can still be reached at $t = (n + 1/2)T_\text{B} \mp \arccos(\tau/2\tau_d)$. In our situations, $|S_{x,y}| \gg |S_y|$. The pseudospin dynamics in the (x, z) plane reveals a topological phase transition. Fig.7(a) shows an example of topological trivial band with $\tau_d < \tau/2$, where the vector $\mathbf{S}(t) = (S_x(t), S_z(t))$ swings periodically around the S_x direction. At $\tau_d = \tau/2$ [Fig.7(b)], $\mathbf{S}(t)$ rotates a full circle in a couple of Bloch periods. For $\tau_d > \tau/2$, Fig.7(c) shows that $\mathbf{S}(t)$ rotates a full circle in a single BO period, reflecting the nontrivial topology of the energy bands. In the phase with non-

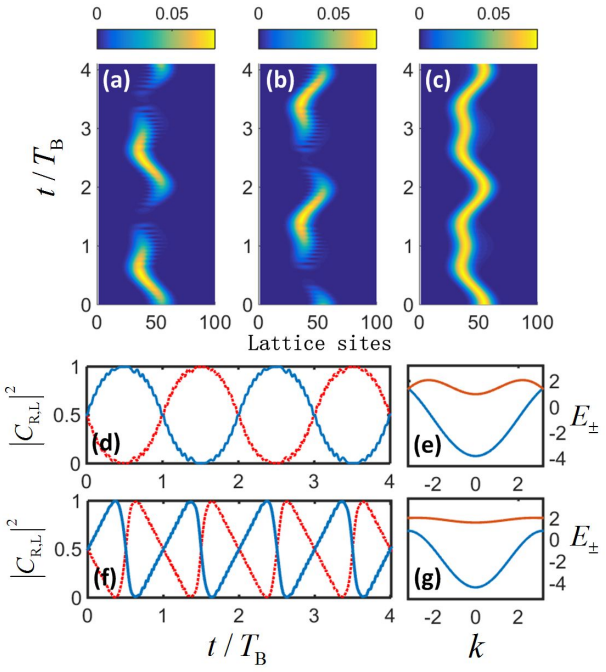

FIG. 6: (Color online) (a-c) The same as in fig.1(a-c) in the presence of diagonal tunneling which equals half of the inter-chain tunneling ($\tau_d = \tau/2 = 0.6$) for magnetic flux $\Phi = 2\phi = 0.5\pi$. (d) The temporal evolution of the density fraction in the left (blue solid curve) and the right (red dotted curve) legs. The oscillating period is doubled. (e) is the lowest two bands $E_\pm$ where the gap is closed at the BZ edges. As a comparison, (f) displays a typical case for $\tau_d > \tau/2$ ($\tau = 1.2$ and $\tau_d = 0.9$) where the oscillating period again equals the BO period. (g) shows that the band gap is reopened.

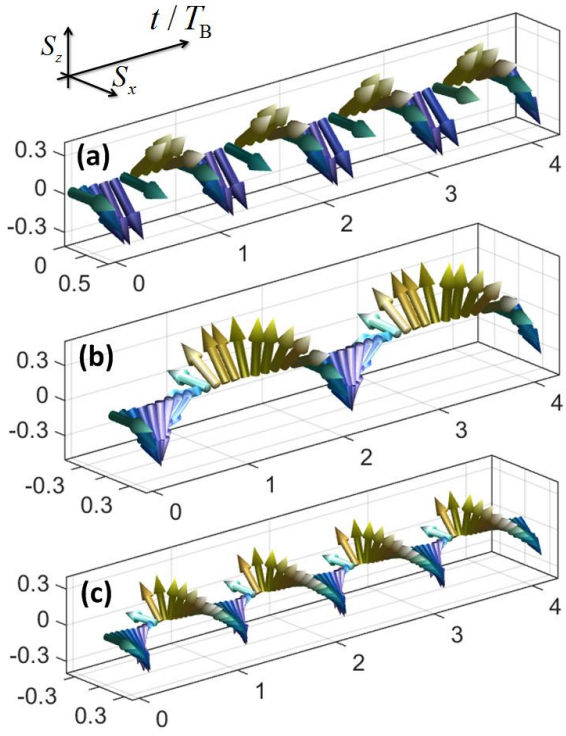

FIG. 7: (Color online) Temporal evolutions of the pseudospin polarization in the chiral BOs for fixed $\tau = 1.2$, $\Phi = 2\phi = 0.5\pi$ and different diagonal hoppings within the Meissner region. (a) $\tau_d = 0.3$. (b) $\tau_d = 0.6$. (c) $\tau_d = 0.9$. The color of the arrows indicate the value of S_z. (a) shows a trivial topology with no spin winding as $\tau_d < \tau/2$. (b) reveals that the spin polarization rotates a full circle (the spin winding once) in two BO periods at the critical point of $\tau_d = \tau/2$, where the band gap is closed (fig.6(e)). (c) exhibits the spin winding once in each BO period in the regime of $\tau_d > \tau/2$, where the band gap is reopened (fig.6(g)).

zero winding number, the pseudospin can be polarized to the positive (negative) S_z direction when $|C_{\rm L}(t)|^2 = 1$ ($|C_{\rm R}(t)|^2 = 1$), which is essentially distinct from the topological trivial phase where $|C_{\rm R,L}(t)|^2 < 1$. Defining $C_{\rm max} = |C_{\rm R,L}(t)|^2_{\rm max}$ and $\tilde{a}_c = a_c(t = nT_{\rm B})$, the Bloch oscillation process can signify the phases in Fig.5. Above (below) the dashed lines, $C_{\rm max} = 1$ ($C_{\rm max} < 1$), corresponding to the topological nontrivial (trivial) phase. On the left (right) side of the solid lines, $\tilde{a}_c < 0$ ($\tilde{a}_c > 0$), corresponding to the Meissner (vortex) phase.

V. EVOLUTION IN THE MOMENTUM SPACE

The broad wave packet in the real space signifies an eigenstate with quasi-momentum k in a semiclassical description. By referring to Ref.[29], the system exhibits features of the Wannier-Stark ladder when a linear force F is applied, with the eigen equation,

$$E_\pm \psi_m(k) + iF\frac{d\psi_m(k)}{dk} = E_m \psi_m(k). \quad (14)$$

Here the eigen energies are $E_m = mF$ ($m = 0, \pm 1, ...$) due to the periodic boundary condition $\psi_m(k \pm 2\pi) = \psi_m(k)$ for a Wannier-Stark state under the quasi-momentum basis. The corresponding eigenstates are

$$\psi_m(k) = \langle k|\psi_m\rangle = \frac{1}{\sqrt{2\pi}} e^{-i\left[mk - \frac{1}{F}\int_0^k E_\pm(k_0)dk_0\right]}. \quad (15)$$

The Bloch oscillation can be derived from the time evolution operator

$$\begin{aligned} U_{k'k}(t) &= \langle k'|e^{-iHt}|k\rangle \\ &= \sum_m \langle k'|\psi_m\rangle e^{-iE_m t}\langle \psi_m|k\rangle \\ &= e^{-\frac{i}{F}\int_k^{k'} E_\pm(k'')dk''} \cdot \delta(k' - k + Ft), \end{aligned} \quad (16)$$

By replacing k with the initial momentum $k = k_0$, we arrive at the dynamics of the quasi-momentum $k(t) \equiv k'$ given by Eq.8.

This result is independent of the band index. Given a positive F, the propagating direction of $|k\rangle$ in the Brillouin zone (BZ) is always from π to $-\pi$. The density distributions in the two chains rely on the time-dependent

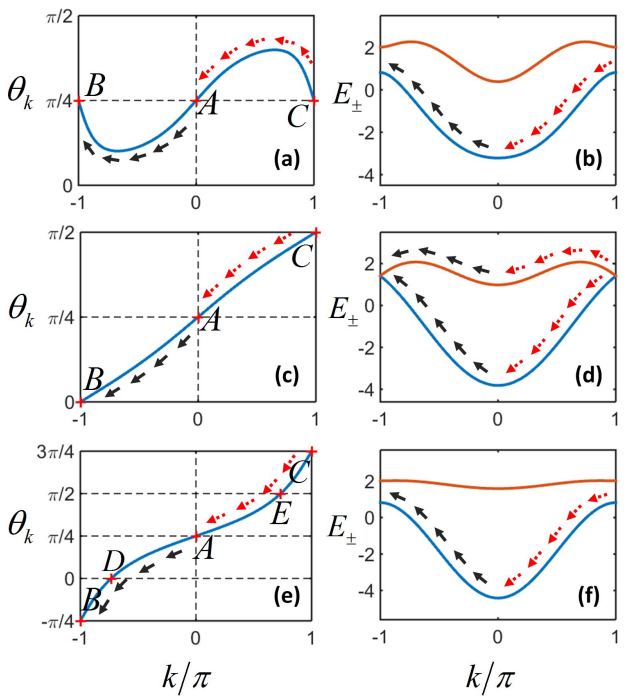

FIG. 8: (Color online) (a,c,e) The values of θ_k versus k from Eq.(12) for three typical cases: (a) $\tau_d < \tau/2$, (c) $\tau_d = \tau/2$ and (e) $\tau_d > \tau/2$, respectively. The corresponding bands are shown in the right panels. The parameters are $\tau = 1.2$, $\Phi = \pi/2$. The initial state with $k_0 = 0$ are labeled by A to represent the state $|k\rangle = \sqrt{2}/2(a_k^\dagger + b_k^\dagger)|0\rangle$. The labels B indicate (a) $|k\rangle = \sqrt{2}/2(a_k^\dagger + b_k^\dagger)|0\rangle$, (c) $|k\rangle = a_k^\dagger|0\rangle$ and (e) $|k\rangle = \sqrt{2}/2(a_k^\dagger - b_k^\dagger)|0\rangle$. The labels C indicate (a) $|k\rangle = \sqrt{2}/2(a_k^\dagger + b_k^\dagger)|0\rangle$, (c) $|k\rangle = b_k^\dagger|0\rangle$ and (e) $|k\rangle = \sqrt{2}/2(-a_k^\dagger + b_k^\dagger)|0\rangle$. The labels D, E in (e) represent the same state as B, C in (c). All above states are restricted to their lower bands. The arrows indicate the evolution of $k(t)$ according to Eq.(8). The evolution for the first and second half of the BO period are specified by black (solid) and red (dashed) arrows, respectively. The band crossing occurs in (d), where the state $|k = (-\pi)^+\rangle_-$ in the lower band connects with the upper band state $|k = \pi^-\rangle_+ = a_k^\dagger|0\rangle$. Similarly, the state $|k = (-\pi)^+\rangle_+ = -b_k^\dagger|0\rangle$ is connected to $|k = \pi^-\rangle_-$.

coefficients $|\cos\theta_k|^2$ and $|\sin\theta_k|^2$ defined by Eq.(12). Figure 8(a,c,e) display the values of θ_k versus k. The arrows indicate the propagating direction of k while the values of k are folded into the first BZ.

We first focus on the critical case of $\tau_d = \tau/2$, where there are two saltation points $k = 0$ and $k = -\pi$ in one Bloch period $T_B = 2\pi/F$. The Bloch period correspond to the ergodicity of quasi-momentum k in the BZ. At $k = 2n\pi$ with $n = 0, \pm1, ...$, the values of $\tan 2\theta_k$ are decided by the sign of k so that

$$\tan 2\theta_k = \begin{cases} \infty, & k = 0^- \\ -\infty, & k = 0^+. \end{cases} \tag{17}$$

At $k = -\pi + 2n\pi$, we have

$$\tan 2\theta_k = \frac{2\tau_d \sin k}{2\sin\phi\cos k}|_{k=-\pi+2n\pi} = \begin{cases} 0^+, & -\sin k = 0^+ \\ 0^-, & -\sin k = 0^-. \end{cases} \tag{18}$$

Note that $|k = 0^+\rangle$ and $|k = 0^-\rangle$ should be the same state as labeled by A in Fig.8(c). It means that the scale of θ_k is bounded to the regime $[0, \pi/2]$. The variation of θ_k is represented by arrows in Fig.8(c,d). In our consideration, the wave packet is initialized by $|k = 0\rangle_-$ in the lower band (with the subscript indicating the band index), *i.e.*, $\theta_k = \pi/4$, thus $\alpha_k^\dagger = \frac{\sqrt{2}}{2}a_k^\dagger + \frac{\sqrt{2}}{2}b_k^\dagger$. The wave packet evolves in the lower band for $t \in [0, T_B/2]$ as shown by the black solid arrows in Fig.8(c). When the eigenstate $|k\rangle_-$ in quasi-momentum space arrives at $|k = (-\pi)^+\rangle_-$, then $\tan 2\theta_k = 0^+$, leading to $\alpha_k^\dagger = a_k^\dagger$. It means that the wave packet completely populates the left chain in real space. Subsequently, the transition for $\tan 2\theta_k$ from 0^+ to 0^- in Eq.(18) occurs. Such transition corresponds to a saltation for θ_k from 0 to $\pi/2$ (k: $(-\pi)^+ \to \pi^-$). However, $\theta_k = \pi/2$ ($k = \pi^-$) implies that $\alpha_k^\dagger = b_k^\dagger$ and $\beta_k^\dagger = a_k^\dagger$ from Eq.(6). To keep the state in the lower band the wave packet need to be suddenly flipped to the right chain, which is just impossible.

We come to the conclusion that the state jumps to the state $|k = \pi^-\rangle_+$ without altering the density distribution. Hence in the second half of BO $t \in [T_B/2, T_B]$, the state begins to propagate in the upper band as indicated by the red dashed solid arrows in Fig.8(d). At $t = T_B$, the state reaches $|k = 0\rangle_+$ with $\tan 2\theta_k$ encountering the saltation from $-\infty$ to ∞ in Eq.(17) and hence we have $\theta_k = \pi/4$, again. The value of θ_k completes a cycle in a Bloch period. However, the state is now in the upper band. An additional Bloch period is needed for $|k = 0\rangle_+$ to return to the initial state $|k = 0\rangle_-$. It means that the full period of the BO doubles that of $\tau_d < \tau/2$. The subsequent evolution of the state is again indicated by the black solid arrows in the upper band and the red dashed arrows in the lower band. For $|k = (-\pi)^+\rangle_+$, we have $\theta_k = 0$ and thus $\beta_k^\dagger = -b_k^\dagger$, while for $|k = \pi^-\rangle_-$, $\theta_k = \pi/2$, thus $\alpha_k^\dagger = b_k^\dagger$ and $\beta_k^\dagger = a_k^\dagger$. In spite of a phase jump of π which has no effect on the physical observable, the state $|k = (-\pi)^+\rangle_+$ is connected to $|k = \pi^-\rangle_-$.

For the case of $\tau_d > \tau/2$, the crossing bands reopen, resulting in topologically nontrivial band structure in contrast to that of $\tau_d < \tau/2$. To get insights into the topological transition, we compare the values of θ_k versus k in Fig. 7(a) and (e). For $\tau_d < \tau/2$, θ_k can reach neither 0 nor $\pi/2$, which means the density always distributes in both chains and the total pseudospin can not be fully polarized. In Fig.8(a) points B and C are the same state $|k\rangle = \sqrt{2}/2(a_k^\dagger + b_k^\dagger)|0\rangle$. For $\tau_d > \tau/2$, however, θ_k reaches 0 and $\pi/2$ at $k = \mp\arccos(-\tau/2\tau_d)$. As indicated by D and E in Fig.8(e). The corresponding states are $|k\rangle = a_k^\dagger|0\rangle$ and $|k\rangle = b_k^\dagger|0\rangle$, respectively. The states labeled by B and C are now different. Since they are states at $|k = \mp\pi\rangle$, the physical observable should be the

same. The only distinction they preserve is a global phase of π. We have state B: $|k=(-\pi)^+\rangle=\sqrt{2}/2(a_k^\dagger-b_k^\dagger)|0\rangle$ and state C: $|k=\pi^-\rangle=\sqrt{2}/2(-a_k^\dagger+b_k^\dagger)|0\rangle$. The lower band in such case is analogous to the Mobius band since there is a phase jump of π between the two states B ($|k=(-\pi)^+\rangle$), C ($|k=\pi^-\rangle$).

VI. BAND TOPOLOGY AND EDGE STATES

To characterize the band topology, we compute the topological invariant. By applying the rotation $(\sigma_x,\sigma_y,\sigma_z)\rightarrow(\sigma_x,\sigma_z,-\sigma_y)$, we get the one-dimensional Hamiltonian of the canonical form

$$\mathcal{H}(k)=\varepsilon(k)+\tilde{\tau}(k)\sigma_x+\kappa(k)\sigma_y, \tag{19}$$

where $\varepsilon(k)=2\cos\phi\cos k$, $\tilde{\tau}(k)=\tau+2\tau_d\cos k$ $\kappa(k)=2\sin\phi\sin k$. As mentioned in ref.[16], for $\Phi=2\phi=\pi$, the Hamiltonian in Eq.19 is analogous to the Su-Schrieffer-Heeger (SSH) model[30, 31]. Rigorously, the two hopping rates in the corresponding SSH model are $J=\tau$, $J'=2\tau_d$ when $k=\pm\pi$. Thus $\tau_d=\tau/2$ leads to the halving of the effective unit cell, resulting in the doubling of the Bloch period as demonstrated in Fig.6(a-d).

The normalized Bloch wavefunction for the lower band is

$$|u(k)\rangle=\frac{1}{\sqrt{2}}\begin{pmatrix}q\\1\end{pmatrix}, \tag{20}$$

with $q=(-\tilde{\tau}+i\kappa)/\lambda$ and $\lambda=\sqrt{\tilde{\tau}^2+\kappa^2}$. The winding number is obtained by

$$\begin{aligned} w[q] &= \frac{i}{2\pi}\int_{\rm BZ}q^{-1}dq=-\frac{1}{2\pi}\int_{\rm BZ}\frac{\kappa\tilde{\tau}'-\tilde{\tau}\kappa'}{\kappa^2+\tilde{\tau}^2}dk \\ &= \frac{1}{2\pi}\arctan(-\frac{\tilde{\tau}}{\kappa})|_{\rm BZ}, \end{aligned} \tag{21}$$

Where we have used the definition of the winding number. Since $q^{-1}=q^*$, this formula can be expressed as

$$w[q]=\frac{i}{\pi}\int_{\rm BZ}\langle u(k)|\partial_k|u(k)\rangle dk\equiv\frac{\varphi_{\rm Zak}}{\pi}, \tag{22}$$

where $\varphi_{\rm Zak}$ is called the Zak phase which is the Berry phase of the one dimensional (1D) version[32]. Eq.(22) shows that $w[q]$ is invariant to a gauge transformation $|u(k)\rangle\rightarrow e^{i\gamma}|u(k)\rangle$ as long as γ is k independent. The last expression in Eq.(21) reveals that the winding number is equivalent to the rotation of θ_k in the BZ. Thus from the above analysis (see Fig.8(a,c,e)), we directly come to the conclusion that $w[q]=0$, $1/2$ and 1 for $\tau_d<\tau/2$, $\tau_d=\tau/2$ and $\tau_d>\tau/2$, respectively. We mention that the topology of a band crossing system is not well-defined. Since the band structure is partitioned into two topologically distinct sectors. The system with diagonal tunnelings is specified by the $\mathbb{Z}_2$ class, which can also be determined by the parity (inversion) symmetry $\mathcal{P}a_k^\dagger=a_{-k}^\dagger$ and time-reversal symmetry ($\mathcal{T}a_k^\dagger=a_{-k}^\dagger$)[33].

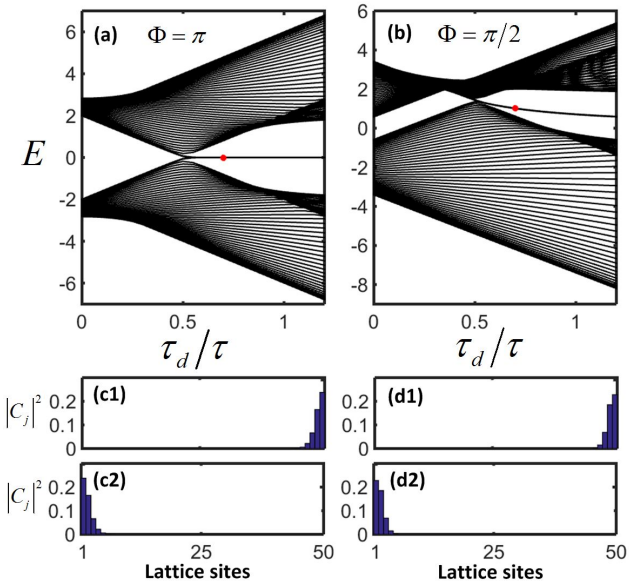

FIG. 9: (Color online) (a,b) The band structure versus τ_d/τ for $\Phi=\pi$ and $\Phi=\pi/2$, respectively. The calculations are carried out for a system of 50 sites along each legs with open boundary conditions. Two degenerate edge states appear when $\tau_d/\tau>0.5$: (c1,c2) are density distributions for the two states marked by red dot ($\tau_d/\tau=0.7$) in (a) and (d1,d2) are density distributions for the marked states in (b). Note that the distribution for the left and right legs are the same, thus only one of the chains is shown.

With open boundary condition, the edge states are always associated with the 1D nontrivial band topology. Such edge states are protected by a chiral symmetry of the bulk Hamiltonian[34], which means the edge states exist if an operator $\mathcal{C}$ can be found such that $\mathcal{C}$ anti-commutes with the bulk Hamiltonian and $\mathcal{C}^2=1$ in the meanwhile. However, as demonstrated in Ref.[35], the existence of edge states is not affected by a term proportional to identity which trivially breaks the chiral symmetry. The Bloch Hamiltonian in our concern can be written as $\mathcal{H}(k)=\varepsilon(k)\hat{1}+\tilde{\tau}(k)\sigma_x-\kappa(k)\sigma_z$. Excluding the first term, we find the chiral symmetry by defining $\mathcal{C}=\sigma_y$. Thus we expect the appearance of edge states when $\tau_d>\tau/2$. Figure 9(a,b) demonstrate the energy bulk and edge states in the open boundary condition. With $\Phi=2\phi=\pi$, $\mathcal{H}(k)$ persist the the chiral symmetry since $\varepsilon(k)=2\cos\phi\cos k=0$. The band structure becomes symmetric, and the edge states have zero energy as predicted by the theory in Ref[34]. With $\Phi=2\phi=\pi/2$, the $\varepsilon(k)$ term induces a shifted dispersion which does not change the band topology. The density distributions for The two degenerate edge states are shown in Fig.9(c1,c2) for the red dot marked in Fig.9(a) and in Fig.9(d1,d2) for the red dot marked in Fig.9(b). Such result exhibits the existence of edge states as band topology arises even in the absence of a chiral symmetry.

VII. DISCUSSION AND SUMMARY

We address some experimental aspects of our work. An array of decoupled optical ladders can be implemented with standing waves that constitute a superlattice potential perpendicular to the arrays. The magnetic flux is readily realized by laser-induced tunnellings[3, 21] while the linear force by accelerating the lattice[36]. By applying a bichromatic superlattice to form the ladder legs and shifting one of the legs along the ladder direction by one site, the diagonal couplings can be enhanced since the corresponding sites belong to the same sublattice. Such ladder configuration resembles the Zeeman field for spin-1/2 systems. With the single-site resolved techniques in optical lattice systems[37–39], measurement of the densities and number fractions in each chain become possible. In Ref.[40], detecting the dynamics of the BOs as well as the quantum walks have been enabled by averaging the densities in parallel 1D lattices. The experiments for ladders require replacing the 1D lattices with two coupled 1D chains. With diagonal tunnelings, the topological phase transition and the period-doubling at transition point can be detected by measuring the density fractions of the two legs. The direct observation of edge states may be implemented with coupled waveguide arrays[41] or in the synthetic dimensions[8]. In optical lattice, a boundary can be generated by setting $\tau_d < \tau/2$ when $j < j_0$ and $\tau_d > \tau/2$ when $j > j_0$. Such configuration supports an edge state located at j_0.

In summary, we have investigated the chiral Bloch oscillations in a bosonic ladder system subjected to an artificial magnetic flux. Detecting the acceleration of the center of the wave packet allows one to identify the Meissner phase and vortex lattice phase. With diagonal coupling, a topological phase transition arises. The Bloch period doubles at the critical point of the phase boundary $\tau_d = \tau/2$ due to the band crossing at the edges of the Brillouin zone. The band topology can be reflected from the dynamical pseudospin texture and the number fractions populated in the two chains. The edge states are demonstrated in the region with nontrivial band topology. Other challenges such as the effect of the linear force in a finite size system, on-site or inter-chain interactions, a boundary of the two domains with distinct topological phases, may require further investigations. We expect that our dynamical method becomes a practical way to identify the quantum phases and topological transitions in condensed matter physics.

This work is supported by the NSF of China under grant Nos. 11774034 and 11374036, and the National Basic Research Program of China under grant No. 2012CB821403.

[1] Y.-J. Lin, R. L. Compton, K. Jimenez-Garcia, J. V. Porto and I. B. Spielman, Nature 462, 628 (2009).
[2] N. Goldman and I. Spielman, Reports on Progress in Physics 77, 126401 (2014).
[3] C. J. Kennedy, W. C. Burton, W. C. Chung and W. Ketterle, Nature Physics 11, 859 (2015).
[4] M. Aidelsburger, M. Atala, S. Nascimbene, S. Trotzky, Y. A. Chen and I. Bloch, Phys. Rev. Lett. 107, 255301 (2011).
[5] M. Aidelsburger, M. Atala, M. Lohse, J. T. Barreiro, B. Paredes and I. Bloch, Phys. Rev. Lett. 111, 185301 (2013).
[6] H. Miyake, G. A. Siviloglou, C. J. Kennedy, W. C. Burton and W. Ketterle, Phys. Rev. Lett. 111, 185302 (2013).
[7] G. Moller and N. R. Cooper, Phys. Rev. Lett. 115, 126401 (2015).
[8] B. Stuhl, H.-I. Lu, L. Aycock, D. Genkina and I. Spielman, Science 349 , 1514 (2015).
[9] C. J. Kennedy, G. A. Siviloglou, H. Miyake, W. C. Burton and W. Ketterle, Phys. Rev. Lett. 111, 225301 (2013).
[10] A. Celi, P. Massignan, J. Ruseckas, N. Goldman, I. B. Spielman, G. Juzeliunas and M. Lewenstein, Phys. Rev. Lett. 112, 043001 (2014).
[11] E. Orignac and T. Giamarchi, Phys. Rev. B 64, 144515 (2001)
[12] S. T. Carr, B. N. Narozhny and A. A. Nersesyan, Phys. Rev. B 73, 195114 (2006).
[13] A. Dhar, M. Maji, T. Mishra, R. V. Pai, S. Mukerjee and A. Paramekanti, Phys. Rev. A 85, 041602(R) (2012).
[14] A. Petrescu and K. Le Hur, Phys. Rev. Lett. 111, 150601 (2013).
[15] A. Tokuno and A. Georges, New Journal of Physics 16, 073005 (2014).
[16] D. Hügel and B. Paredes, Phys. Rev. A 89, 023619 (2014).
[17] R. Wei and E. J. Mueller, Phys. Rev. A 89, 063617 (2014).
[18] A. Petrescu and K. Le Hur, Phys. Rev. B 91, 054520 (2015).
[19] M. Piraud, F. Heidrich-Meisner, I. P. McCulloch, S. Greschner, T. Vekua and U. Schollwöck, Phys. Rev. B 91, 140406(R) (2015).
[20] S. Kessler and F. Marquardt, Phys. Rev. A 89, 061601 (2014).
[21] M. Atala, M. Aidelsburger, M. Lohse, J. T. Barreiro, B. Paredes and I. Bloch, Nature Physics 10, 588 (2014).
[22] Y.-J. Lin, K. Jimenez-Garcia and I. B. Spielman, Nature 471, 83 (2011).
[23] Y. V. Kartashov, V. V. Konotop, D. A. Zezyulin and L. Torner, Phys. Rev. Lett. 117, 215301 (2016).
[24] W. Tschischik, R. Moessner and M. Haque, Phys. Rev. A 92, 023845 (2015).
[25] H. Zhai, International Journal of Modern Physics B 26, 1230001 (2012).
[26] B. N. Narozhny, S. T. Carr and A. A. Nersesyan, Phys. Rev. B 71, 161101(R) (2005).
[27] G. Roux, E. Orignac, S. R. White and D. Poilblanc, Phys. Rev. B 76, 195105(2007).
[28] M. Holthaus and D. W. Hone, Philosophical Magazine Part B 74, 105 (1996)
[29] T. Hartmann, F. Keck, H. J. Korsch and S. Mossmann, New Journal of Physics 6, 2 (2004).
[30] W. P. Su, J. R. Schrieffer, and A. J. Heeger, Phys. Rev. Lett. 42, 1698 (1979).

[31] A. J. Heeger, S. Kivelson, J. R. Schrieffer and W. P. Su, Rev. Mod. Phys. 60, 781 (1988).
[32] J. Zak, Phys. Rev. Lett. 62, 2747 (1989).
[33] S. Ryu, A. P. Schnyder, A. Furusaki and A. W. W. Ludwig, New Journal of Physics 12, 065010 (2010).
[34] S. Ryu and Y. Hatsugai, Phys. Rev. Lett. 89,077002 (2002).
[35] P. Delplace, D. Ullmo, and G. Montambaux, Phys. Rev. B 84, 195452 (2011).
[36] C. Sias, H. Lignier, Y. P. Singh, A. Zenesini, D. Ciampini, O. Morsch, and E. Arimondo, Phys. Rev. Lett. 100, 040404 (2008).
[37] W. S. Bakr, J. I. Gillen, A. Peng, S. Fölling and M. Greiner, Nature 462, 74 (2009).
[38] J. F. Sherson, C. Weitenberg, M. Endres, M. Cheneau, I. Bloch and S. Kuhr, Nature 467, 68 (2010).
[39] M. F. Parsons, F. Huber, A. Mazurenko, C. S. Chiu, W. Setiawan, K. Wooley-Brown, S. Blatt and M. Greiner, Phys. Rev. Lett. 114 (21), 213002 (2015).
[40] P. M. Preiss, R. Ma, M. E. Tai, A. Lukin, M. Rispoli, P. Zupancic, Y. Lahini, R. Islam and M. Greiner, Science 347, 1229 (2015).
[41] Y. Plotnik, M. C. Rechtsman, D. Song, M. Heinrich, J. M. Zeuner, S. Nolte, Y. Lumer, N. Malkova, J. Xu, A. Szameit, Z. Chen and M. Segev, Nat. Mater. 13, 57 (2014)